Song, L.; Wang, L.; Zhang, T.; Lin, Y.; Pyczak:

Microstructure and phase transformations of ωo-Ti4Al3Nb based alloys after quenching and subsequent aging at intermediate temperatures.

In: Journal of Alloys and Compounds. Vol. 821 (2020) 153387.

First published online by Elsevier: 13.12.2019

https://dx.doi.org/10.1016/j.jallcom.2019.153387

Microstructure and phase transformations of ω_o-Ti_4Al_3Nb based alloys after quenching and subsequent aging at intermediate temperatures

Lin Song[a,b]*, Li Wang[b]*, Tiebang Zhang[a], Junpin Lin[c], Florian Pyczak[b]

[a]State Key Laboratory of Solidification Processing, Northwestern Polytechnical University, Xi'an, Shaanxi 710072, China

[b]Institute of Materials Research, Helmholtz-ZentrumGeesthacht, Max Planck-Str. 1, Geesthacht, D-21502, Germany

[c]State Key Laboratory for Advanced Metals and Materials, University of Science and Technology Beijing, Beijing 100083, China

Corresponding authors: Lin Song (songlin@nwpu.edu.cn, lin.song@hzg.de), Li Wang (li.wang1@hzg.de)

Abstract

The existence of ω_o (ordered ω) phase in TiAl alloys in different compositions at intermediate temperatures has been widely reported. In this study, the phase transformation behaviors of ω_o-based alloys at 750-900 ℃were studied by electron microscopy. It is found that fine-grained microstructures mainly composed of $\gamma+\omega_o$and a tiny amount of $\alpha_2$phase precipitated in the alloys quenched from high temperatureduring aging. Twinsform inα_2 phase after aging, which is analogous to observations reported in deformed TiAl alloys. The γ phase precipitatesoriginate from the stacking faults of α_2 laths and grow up by coarsening at 750 ℃. Semi-coherent interfaces between γ and ω_o phases are formed and a high density of stacking faults can be observed inside the α_2 laths. At higher temperatures, the direct nucleation of γ phase from the ω_o/β_o matrix becomes active. Various orientation relationships are found between ω_o, γ and α_2 phases, leading to a number of grain clusters having smooth interfaces inbetween. In addition, the effects of Ta, V and Zr on the microstructure are investigated. The effect of these elements on the stability of the ω_o phase is not as obvious as reported for some other elements.

Keywords: TiAl alloys; precipitation; microstructure; phase transitions; transmission electron microscopy

1. Introduction

The existence of ω_o(ordered ω) phase has been confirmed in many Nb containing TiAl-based alloys, which are promising high temperature structural materials used for aeroengines [1-4]. It is commonly known that the ω_o phase usually precipitates inside the β_o phase at lower temperatures during cooling [5-6].Besides β_o phase, recently it is found that the ω_o phase could also precipitate in the lamellar colonies after long-term annealing or creep test via$\alpha_2\rightarrow\omega_o$or $\beta_o\rightarrow\omega_o$phase transformations, making it important for the microstructural stability and mechanical properties. The precipitation of ω_o phase is a common phenomenon in various TiAl-based alloys with different compositions, especially when a high amount of Nb is add [4, 7-9]. Moreover, phase diagram calculation also indicates that there is an$\omega_o$phase

region at lower temperatures in the ternary Ti-Al-Nb system [10]. Therefore, the ω_o phase is expected an equilibrium phase in high Nb-containing TiAlalloys and thus it is unavoidable during long-term service of these alloys.Since the lamellar colonies are composed of alternating γ and α_2 laths, when the $\alpha_2 \rightarrow \omega_o$ phase transformation happens in the lamellar colonies, phase transformation between ω_o and γ phases is occasionally reported as a side effect of the growing up of ω_o phase,yeta direct $\omega_o \rightarrow \gamma$ transformation was not observed [11]. On the other hand, the $\beta_o \rightarrow \gamma$ phase transformation was reported by several researchers in various alloy compositions, following the orientation relationship $<111>_{\beta o}//<110>_{\gamma}$; $\{110\}_{\beta o}//\{111\}_{\gamma}$ [12-14]. As a result, by a subsequentβ_o to ω_o phase transformationa connection between γ and ω_o phases is possible. For alloys with lowerNb content or other alloying elements, the appearance of ω_o phase varies with the composition because even a small amount of a certain alloying element can have a significant effect on the solvus temperatureof ω_o phase. For instance, Mo, Mn and W have a strong effect on inhibiting theω_o phase formation whereas Ni promotes the ω_o phase formation [15-17]. In the Zr and Hf containing TiAl alloys, the ω_o phase formation was also observed [18-20], whereas the comparison between the other elements was not specifically addressed. The effects of other elements, such as Ta and V, which are common alloying elements of TiAl alloys, are not clearly known.

To investigate the ω_o phase, an effective way is to use the nominal composition alloy Ti_4Al_3Nb (Ti-37.5Al-12.5Nb, all the contents are in atomic percent at.%). Unfortunately, few researchers have focused on this topic, thus the available data is limited. An earlier report of Bendersky et al. [21] indicated that single ω_o phase could not be obtained in the nominal composition alloyeven after long-term heat treatment. In fact, the precipitation of γ and α_2 phase was observed and the orientation relationship between these three phases is: $<0001>_{\omega o}//<11\bar{2}0>_{\alpha 2}//<110>_{\gamma}$; $\{11\bar{2}0\}_{\omega o}//\{0001\}_{\alpha 2}//\{111\}_{\gamma}$. This orientation relationship is frequently reported [4, 8, 11-12]. The authors also indicated that there could be a phase transformation between γ and ω_o phase. Ye et al. [22] found that the α_2 phase grew faster than the ordered ω_o phases in the β_o matrix during cooling, and a variant selection process of the ω_o phase existed at the α_2/β_ointerfaces. Our previous results showed that in thealloy Ti-34Al-13Nb, the precipitation of $\alpha_2$phase introduced a microstructure similar to those reported in β-Ti alloys but the matrix was in fact theω_o phase [23]. In general, in Ti-Al-Nb ternary alloys close to the Ti_4Al_3Nb composition, fine-grained microstructures are easy to obtain by simple heat treatment due to the variants formation mechanism in the $\beta_o \rightarrow \omega_o$ and $\beta_o/\omega_o \rightarrow \gamma/\alpha_2$ phase transformation processes. Nevertheless, a detailed study on the interface structures, microstructure evolution and composition redistribution is still lacking.

In the present study, the microstructures of Ti_4Al_3Nb based alloys after fast cooling and subsequent aging at different temperatures are examined by scanning electron microscopy (SEM) and transmission electron microscopy (TEM). In addition, Ta, V and Zrwere addedto the Ti_4Al_3Nb alloyto explore the effect of these elements on the ω_o phase formation.

2. Experiments

Button ingots of four alloys: Ti-37.5Al-12.5Nb (Ti_4Al_3Nb), Ti-37.5Al-12.5Nb-2Ta (Ti_4Al_3Nb-2Ta),Ti-37.5Al-12.5Nb-2V (Ti_4Al_3Nb-2V), and Ti-37.5Al-12.5Nb-2Zr (Ti_4Al_3Nb-2Zr)were prepared by vacuum arc melting using the pure elements as raw materials. Each button ingot was flipped and re-melted for 10-14 times. After the melting, the ingots were homogenized at 1250 ℃ for 2 h followed by water-quenching. The original as-quenched microstructure was characterized by room temperature high-energy X-ray diffraction analysis utilizing the P07 high-energy materials science beamline (beam size 0.5×0.5 mm^2 and wavelength 0.124 Å) operated by Helmholtz-ZentrumGeesthacht at PETRA III of DeutschesElektronen-Synchrotron (DESY) in Hamburg, Germany.Then, all the ingots were cut into pieces for subsequent aging treatments. For the Ti-37.5Al-12.5Nb alloy, heat treatmentswere conducted at 750 ℃ for 200 h and 800/900 ℃ for 100 h. For the other three alloys, the agingwas conducted at 800 and 900 ℃ for 100 h. All the samples were water-quenched after the treatment. Before preparing the samples for electron microscopy observation, a 2 mm surface layer was removed from the samples. Specimens for scanning electron microscopy (SEM, GEMINI 1530, Zeiss, Germany) observation were cut from the center of the heat-treated samples and grinded by sandpaper, then vibration polished. Backscattering electron (BSE) mode was used for SEM observation at an acceleration voltage of 15kV and a working distance of 7mm. Disks for TEM observation were mechanically grinded to 0.1mm in thickness and prepared using the conventional twin-jet polishing method in a solution of 5%perchloric acid, 35%butan-l-ol, and 60% methanol at 28V and -45℃ until electron transparent. Conventional TEM and high-resolution TEM (HRTEM) investigations were conducted on a Cs-corrected FEI Titan 80-300 field emission TEM (FEI company, USA) operating at 300kV. Fast Fourier transformed (FFT) images were obtainedwith theDigitalMicrograph software. Elemental analysis was performed using energy dispersive X-ray spectroscopy (EDX) in a Philips CM200 TEM operated at 200 kV. The EDX spectrums were collected using an Oxford instrument X-mas EDX system and analyzed withtheOxford Inca software. Each result presented here is an average value of at least five point measurements at different locations.

3. Results and discussion

3.1 Phase constitution of Ti_4Al_3Nb alloy at different temperatures

The microstructure of the Ti_4Al_3Nb alloy after quenching is shownin Figure 1.Figure 1aexhibits a uniform composition and a coarse-grained matrix. Similar microstructures are obtained in the Ta, V and Zr containing alloys (not shown here), indicating that all the alloys are in the single β(or β_o) phase region at 1250 ℃. The room-temperature synchrotron radiation X-ray diffraction pattern is shown in Figure 1b. Besides the β_o phase, diffusive diffraction spots of ω-related phase are observed, indicating certain amount of ω-related phase is induced by quenching, which is in accordance with that observed by TEM [5, 12, 23]. The microstructures afteragedat various temperatures are shown in Figure 2recorded by

SEM. The particles in dark contrast are γ grains. The phase constitution, as confirmed by the following TEM observation, mostly consists of γ precipitates embedded in the $\omega_o$matrix and a small amount of α_2 phase. However, the α_2 phase can hardly be distinguished in the SEM images due to its small size. In general, the microstructures after 750 ℃/200 h and 800 ℃/100 h are similar. In the sample heat-treated at 750 ℃, it can be seen that the microstructure is very fine-grained with an average grain size of the γ phase of less than 500 nm. The sizes of the $\omega_o$grains are also very small, with less than 1μm. Similaror slightly smaller grain sizes can also be seenin the sample aged at 800 ℃ for 100 h, indicating that during the 200 h aging at 750 ℃ the γ grains kept growing. Interestingly, in the magnified image inserted in Figure 2b, some fish-bone like structures can be observedin various directions. These are in fact γ grains growing out of the α_2 laths, which will be discussed in more detail in the next section. In the sample aged at 900 ℃, it is obvious that the γ grains have grown up to larger sizes, namely 1-2 μm. Correspondingly, the sizes of the matrix regions between the γphase have also increased. By examining in TEM, it can be confirmed that the matrix is still ω_o but not β_o phase. It should be noted that the fish-bone like structures diminished in the samplesaged at 800 and 900 ℃, indicating different growth mechanisms of the γ phase.

Similar microstructures have been reported in our previous workin a different alloy composition [23]and in [13], where the β_o phase was the matrix and a high amount of Mo was added to stabilize the β_o phase. The fine-grained microstructure resulted from the various orientation relationships between these phases, which can be explained as follows. The primary microstructure after fast cooling is a coarse-grainedβ_o matrix withω-related phase exists in the microstructure (Figure 1). In addition, a large amount of vacancies is expected in the initial microstructure, which can serve as nucleation sites for the heterogeneous nucleation.During aging, the γ and α_2 phase precipitation starts and the ω_o phase also begins to grow. For the γ phase, a direct nucleation was observed in other alloys in the β_o matrix, following the commonly reported Kurdjumov–Sachs orientation relationship $\{110\}_{\beta o}//\{111\}_{\gamma}$; $<111>_{\beta o}//<110>_{\gamma}$ [12-13]. Thus, 48γvariants can formduring the $\beta_o \rightarrow \gamma$ phase transformation even if the tetragonality of the $L1_0$ structure is not considered. Although the γ phase is in the $L1_0$ structure and thus the $<110]_{\gamma}$ and $<101]_{\gamma}$ directions are different in atomic arrangements, both of these zone axis can be parallel with $<111>_{\beta o}$ with a small misfit [13]. Moreover, it seems there is no preferential variant selection of the γ phase due to the different atomic arrangements based on the following TEM observations. For the α_2 phase, the well-known Burgers orientation relationship $\{110\}_{\beta o}//\{0001\}_{\alpha 2}$; $<111>_{\beta o}//<11\bar{2}0>_{\alpha 2}$ will be assumed, leading to 12 possible α_2 variants form in a single β_o grain. Moreover, as imaged in the insert of Figure 2b, the α_2 to γ transformation happened. As explained in [24-25], 6 possible variants of γ phase can be generated from a single α_2 lath. For the above mentionedreasons, a large number of possible γ variants can form in the β_o matrix during aging. In addition, considering that4 variants of ω_o phase can be created by the $\beta_o \rightarrow \omega_o$ transformation, the matrix is further refined. On the other hand, the effects of ω_o phase on the γandα_2 phase formation are still not

clear. It is commonly assumed that the ω phase promotesthe αphase formation in disordered alloys and the nucleation sites are usually at the β/ω interface [26]. If the β_o/ω_o interface plays a similar role, the nucleation sites and variant selection mechanism are more complicated. All these effects cause a fine microstructure after the aging. This is slightly different from the situation reported by Erdely et al. [13], where the γ phase grains precipitate in a coarse-grainedβ_o matrix without ω_o phase.

3.2 Phase transformation mechanisms at 750 ℃

The detailed characteristics of the phase transformation at 750 ℃are shown in Figures 3-6. In Figure 2e, a large α_2 lath at the grain boundary of the primary β_o phase has decomposed into an$\alpha_2+\gamma$ structure. This phenomenon is commonly observed in all the aged samples. The long α_2 lath is formedby the β_o to α_2 transformation at the grain boundaries and follows the Burgers orientation relationship with a β_o orientation on one side of the grain boundary, which is also observed in [27]. As can be seen in Figure 3a, the γ phase formed inside the α_2 lath has grown up mostly towards one side of the former β_o matrix (which is now the polycrystalline ω_o matrix). Only occasional γgrains grow into the other side. Furthermore, the γ grains always grow up in pairs in the true twinning orientation relationship (as shown in the enlarged image in Figure 3b). This phenomenon was also observed in [28], in which a quenched high Nb-containing TiAl alloy was subsequently annealed at 800 ℃. As described above, there are different variants of γ phase formed in the α_2 phase, whereas the true twinning relationship is the one of the lowest interface energy [1]. It is inferred that with the growth of the γ phase, the strain field around the γ grain can become increasingly larger since the orientation relationship between γ and ω_o is always kept: $\{11\bar{2}0\}_{\omega o}//\{111\}_\gamma$; $<0001>_{\omega o}//<110>_\gamma$. Thus, a grain in the twining orientation can grow up preferentially to reduce the strain field and make the strain distribution more symmetrical (shown in Figure 5). A similar situation is also observed in the α_2 laths in the ω_o matrix. Figure 3c depicts such an example. However, the α_2 phase has mostly transformed to γ phase while the remaining α_2 phase is with lots of stacking faults, which can also be seen in the large α_2 laths in Figure 3b.Besides, isolated γ phase appears within the ω_o matrix, indicating a direct ω_o to γ transformation, as shown in Figures 3a and 3c. Zhang et al. [29] suggested that the γ precipitates exhibit acicular morphology while Erdely et al. [13] mentioned the disc-like shape of γ phase. The shape of γ phase in the present alloy is in fact analogous to that reported by Bendersky et al. [21], i.e., the grains are elongated along the $<110>_\gamma$ directions while appearing ellipsoidalwhen viewed along this direction. Nevertheless, the present samples are the aged ones. It is inferredthat certain interface structures,which can form at the beginning of γ phase formation, only partly remain after long-term aging.

Figure 4shows a group of HRTEM images obtained at the interfaces in the 750 ℃aged sample. In the middle of Figure 4a, a pair of α_2 grains isshown, where both grains are in a very special “twin-like” orientation relationship. As can be seen in the FFT image of zone I, the two $[11\bar{2}0]_{\alpha 2}$ zone axes share the same $(20\bar{2}1)$ plane in the diffraction pattern, and the diffraction spots are symmetric with respect to the $(20\bar{2}1)$ mirror plane. This orientation relationship of α_2 phase stems from the$\beta_o\rightarrow\alpha_2$ or $\omega_o\rightarrow\alpha_2$ phase

transformation. A slight tilt was introduced between two α_2 variants to accommodate the lattice misfit to a low-energy [$11\bar{2}0$]/60° condition [23, 26, 30]. Since the α_2 phase will transform to γ phase during aging, each α_2 phase can generate a group of γlaths based on the orientation relationship $\{0001\}_{\alpha2}//\{111\}_{\gamma}$; $<11\bar{2}0>_{\alpha2}//<110>_{\gamma}$. Thus, γ grains in different orientations are created, as shown on the left and right side of Figure 4a.The γ zone II has developed from α_{2T} while in zone III the two γ grains have developed from α_2. Also, a 120° rotational boundary is created between the two γ grains at the left side (FFT of zone III), which is a common phenomenon during the α_2 to γ transformation. Furthermore, the growth of γtakes place by a ledgemechanism. A one-atomic layer disconnection between theγ and α_2 grainsis observed in the magnified image inserted, indicating that the γ phase grows layer by layer by a dislocation climb process [31-32], which is also indicated by the arrows in Figure 3b. Thus a smooth interface is remained between γ and α_2. Meanwhile, the interface between the γ zone II and $\alpha_2$containsmany ledges. The FFT image of zone II implies that in fact $(020)_{\gamma II}$ is nearly parallel with $(0001)_{\alpha2}$. The misfit between $(020)_{\gamma II}$ and $(0001)_{\alpha2}$ is approximately 16.8%, which is much higher than the 1.4% between $(111)_{\gamma II}$ and $(0001)_{\alpha2}$ ($d_{(0001)\alpha2}$=0.493 nm, $d_{(111)\gamma}$=0.243 nm and $d_{(020)\gamma}$=0.211 nm obtained from the FFT pattern). Theoretically, the formerone can be very common because it is generated by the crystallographic relationship in the $\beta_o/\omega_o \rightarrow \alpha_2 \rightarrow \gamma$ transformation sequence. Figures 4b-d show the interface morphologies between the α_2/γ laths and the surrounding ω_o matrix. In Figure 4b, the α_2 lath has transformed into nano-sized α_2/γ lamellar structures.Usually, the 6 variants of γ phase should have the same probability to nucleate if they are formed independently. However, most of the γ laths in the lamellar structure are in an identical orientation $<101]_{\gamma}$, which is the same as that of γ zone I and depicted in the FFT. Only a small amount of segments (labeled as "γ_{II}") are in a different orientation. This is more clearly seen in Figure 4c, where two larger γ laths are in the same orientation, indicating that variants in a certain orientation are favorable toform during the $\alpha_2 \rightarrow \gamma$ transformation. As shown in the FFT of zone I and II in Figure 4b, the close-packed planes of $(11\bar{1})_{\gamma}$are parallel with the close-packed plane of $(11\bar{2}0)$ in the ω_o phase. Meanwhile, the $(\bar{1}11)_{\gamma}$ plane is theoretically 10.5° away from the $(\bar{2}110)_{\omega o}$ plane because the angles formed by equivalent $\{111\}_{\gamma}$planes and $\{11\bar{2}0\}_{\omega o}$planes are 70.5° and 60° respectively.Moreover, the interplanar spacing of $(\bar{2}110)_{\omega o}$ at this position is 0.243 nm which is exactly the same as that of $(\bar{1}11)_{\gamma}$. Thus it is expected that some misfit dislocations should exist along these planes to accommodate the angle deviation, which is observed in practice in Figure 4c. Comparing the HRTEM image of these dislocations to that shown in [1, 33], the Burgers vector is expected to be the one of $a\frac{1}{2}<110]$ordinary dislocation in γ phase of edge type. These edge dislocations at the interface can climb when thermally activated so that the successive climb of the dislocation array will lead to the $\omega_o \rightarrow \gamma$ phase transformation at the interface. The dislocations can serve as diffusion channels as well for the composition change. Therefore, the γ phase can grow from theω_o phase during aging by a relative slow process (controlled by dislocation climb and diffusion) while a semi-coherent interface is kept. This explains the morphology observed Figure3, and the

increasing grain sizes of γ after prolonged aging timein Figure 2b. It should be noted that since fourω_o phase variants are generated from the β_o to ω_o phase transformation, the α_2/γ lamellar structure can connect with an ω_o grain in another orientation. As shown in the zone III in Figure 4b, where the $[20\bar{2}1]\omega_o$ zone axis is indexed, indicating the second orientation relationship $[20\bar{2}1]\omega_o//[11\bar{2}0]\alpha_2$; $(0\bar{1}12)\omega_o//(0001)\alpha_2$[34]. The interface between this ω_{o2} and the lamellar structure is still matching well as this orientation relationship also has a low misfit value, which can be accommodated by the lattice distortion of the numerous α_2/γ laths in the long range, as shown in the upper part of Figure 4b.

A large number of stacking faults exist in the α_2 laths, as shown in Figure 4c,which can serve as nuclei of the γ phase. The rectangular area is enlarged on the right. As indicated by the arrow heads, the "ABC" stacking sequence of γ phase is visible among several α_2 stacking sequences of "ABAB". The borders of these alternating stacking sequences are stacking faults. In fact, a stacking fault in the α_2 structure, which alters the atomic stacking from "..ABAB.." to "..ABCAB..", can be seen as a possible nuclei of γ phase provided diffusion is active to adapt the different chemical compositions of the two phases. Unfortunately, the stacking fault energy of α_2 phase in the present case is unknown. Some reports indicate that the stacking fault energy of α_2 on {0001} planes is relatively low [1, 35], whereas in this study the α_2 phase is off-stoichiometric and Nb atoms areadded. Despite of this, it is reasonableto assume that the stacking fault energy of α_2 phase in the present alloy is still very low. The alternating stacking sequence may have some positive effects on the matching with the surrounding ω_o matrix. Except for the leading partial dislocations of the stacking faults, few misfit dislocation are observed at the $\omega_o/\alpha_2/\gamma$ interface, which is not the case at the ω_o/γ interface as depicted above. Figure 4d shows another interesting interface configuration. A γ grain has formed a continuous interface with the ω_o matrix (zone I, $(11\bar{2}0)_{\omega o}//(11\bar{1})_\gamma$). Also, an interface with numerous misfit dislocations exists between γ and the α_2/γ lamellar structure (zone II), indicating that this γ grain is formed from the matrix rather than the lamellar colony on the right. This makes the interface being accommodated by an array of dislocations to match the $(200)_\gamma$ and $(0001)_{\alpha 2}/(11\bar{1})_\gamma$. In other words, this interface can be explained as a tilting boundary of γ phase with a tilt angle of around 55° along a $<011]_\gamma$ direction. Because the γ grain comes from the ω_o matrix its $(11\bar{1})_\gamma$ plane is parallel with $(11\bar{2}0)_{\omega o}$; meanwhile, the $(0001)_{\alpha 2}/(11\bar{1})_\gamma$ planes of the lamellar colony are parallel with $(\bar{2}110)_{\omega o}$.Thus, a 60° deviation is created between the $\{111\}_\gamma$ planes on the two sides. This means that even if the γ grains are formedby different mechanisms, the interfaces between them can also be of relative low misfit.

The final stage of $\alpha_2 \rightarrow \gamma$ phase transformation is shown in Figure 5. Two γ grains in true twinning relationship are observed with a ledged twinning interface. The ledges left at the interface are probably a result of the ledge movement during the phase transformation. The interfaces formed by γ grains and the ω_o phase are similar to that described in Figure 4c while a coherent interface between ω_o and α_2 remained. This result suggests that the volume fraction of α_2 phase could further decrease if the aging treatment is carried on, and some isolated γ grains can also be a result of $\alpha_2 \rightarrow \gamma$ transformation, where

the α_2 phase has fully decomposed. From Figures 4 and 5, it can be seen that no intermediate orthorhombic phase is observed in the $\alpha_2 \rightarrow \gamma$ transformation. The reason can be attributed to the higher aging temperature, since the orthorhombic phase was usually reported at lower temperatures [36].

The twin-like morphology of α_2 phase is frequently observed, even though most of the $\alpha_2$grains have transformed to lamellar structures. Figure 6a shows three α_2 grains where the one in the middle is in twin relationship with respect to the other two. As shown in the selected area diffraction (SAD) pattern, $(20\bar{2}1)$ serves as the mirror plane and the diffraction spots of $(20\bar{2}1)$ in the twined grains are fully overlapped. Since this kind of morphology is observed not only in the aged state but also in the deformed state, the existence of α_2 phase twinning should be reconsidered carefully. In the deformed high Nb-containing alloy, we have observed deformation twins in α_2 phase, which had exactly the same twining elements as in the present case [37]. However, deformation induced twins are usually small and accompanied by a high density of stacking faults. In thisaged state, although the stacking faults are observed as well, these defects are in fact precursors of γ nucleation but not induced by stress. In a Ti-34Al-13Nb alloy, the twin-like morphology of α_2 phase was more widely formed due to the lower Al content. The$\alpha_2$grainswere elongated along the $\{20\bar{2}1\}$ planes which looked much more like annealing twins [23]. Regardless of the formation mechanism, the resultantmorphology can be perfectly explained by twinning, as the twinning elements $K_1=(20\bar{2}1)$, $K_2=(20\overline{23})$, $\eta_1=[\bar{1}014]$ and $\eta_2=[\bar{3}03\bar{4}]$ are essentially identical to that of the disordered α phase [38]. Thus, to some extent, one can say that the twinning of α_2 phase can be created by both heat treatment and deformation. HRTEM images of the twinning interface are shown in Figures 6b and c. A straight $(20\bar{2}1)$ interface is formed and occasionally some stacking faults causing "ABC" stacking are found (marked by arrows in Figure 6c). The twinning interface structure as well as the related stacking fault activation mechanism would be an interesting future research topic in the ordered structure of $D0_{19}$-α_2.

3.3 Phase transformation mechanisms at 800 and 900 ℃

As shown in Figure 2, the fish-bone like structures in the sample aged at 800 and 900 ℃ disappeared, indicating the direct nucleation of γ phase and a decrease in thevolume fraction of α_2 phase. The TEM images of the microstructure aged at 800 and 900 ℃are shown in Figure 7. Comparing Figure 7a and b, except for the apparent increase in the grain sizes of all the phases, no further difference can be seen between these two temperatures. Thus, the sample aged at 900 ℃was used for further investigation. In Figure 7b, the sizes of the ω_o variants increased to 1-2 μm and the γ phase tends to form clusters of grains with each of the grains having a $<110>_\gamma$ zone axis parallel with $[0001]\omega_o$. As indicated by Bendersky et al. [21], the γ phase is still stable even at 1100 ℃. However, the phase equilibrium is different from the phase diagram indicated by Witusiewicz et al. [10], where an$\alpha_2+\gamma$ phase region is predicted in this alloy composition. Considering that 100 h may be still not enough to reach the equilibrium state, the equilibrium phase composition can be $\omega_o+\gamma$ with a trace amount of α_2 phase (less than 5%) at 800 and 900 ℃. Figures 7c and d show two typical morphologies of α_2 phase in the sample

aged at 900 ℃: i) Three α_2 phase grains can form a triangle area with the grains are connected end to end (Figure 7c); ii) a triple junction can be formed by three α_2 grains while a smooth interface is created by neighboring α_2 grains (Figure 7d).These two configurations are identical to those reported in our previous research [23]. Thisα_2 phase has formed based on the $\{0001\}_{\alpha2}//\{11\bar{2}0\}_{\omega o}$; $<11\bar{2}0>_{\alpha2}//<0001>_{\omega o}$ orientation relationship, in which three α_2 variants can form from three groups of $\{11\bar{2}0\}_{\omega o}$ planes. Besides, some γ grains are present in the α_2 phase, which is probably due to the higher Al content in the present alloy composition compared to that of [23]. The orientation relationships between the γ and α_2 phase is also the same as that shown in Figure 4.

The magnified image of a γ grain cluster is shown in Figure 8a, which is taken along the $[0001]_{\omega o}$ direction. After examining the SAD patterns of each grain, two α_2 grains are found within this cluster and they are in the same orientation. A γ grain formed between the two α_2 grains following the orientation relationship $(0001)_{\alpha2}//(11\bar{1})_{\gamma}$; $[11\bar{2}0]_{\alpha2}//<101]_{\gamma}$. The SAD pattern of zone I is shown in the insert, which implies the orientation relationship of $(11\bar{2}0)_{\omega o1}//(11\bar{1})_{\gamma}$; $[0001]_{\omega o1}//<101]_{\gamma}$. On the other hand, the SAD pattern of zone II on the right indicates the orientation relationship of $(2\bar{1}\bar{1}0)_{\omega o2}//(111)_{\gamma}$; $[02\bar{2}1]_{\omega o2}//<0\bar{1}1]_{\gamma}$. In fact, the change in the orientation of ω_o is due to the different ω_o variants [21], therefore, taking the orientation of ω_{o1}into consideration, the $(111)_{\gamma}$ plane would be in principal parallel with $(1\bar{2}10)_{\omega o1}$. This means these two γ grains are in fact originated from the two ω_o grains with their $\{11\bar{2}0\}_{\omega o}$ planes 60° away from each other, as indicated by the circles in the SAD of zone I. In addition, the SAD pattern obtained from zone III shows a typical 120° rotational variant of γ phase [25]. As a result, the γ grains observed here can be grouped into three variants, indicating that various orientations can be generated in one grain cluster that is composed of α_2 andequiaxedγ grains. Although there is a small difference in the misfits between different $<110>_{\gamma}$directions and $<0001>_{\omega o}$, it seems there is no strong preference in the γ variants formation at a certain location. Similar results are also shown in Figure 8b, where two separated γ grains are found in a twin relationship. As different variants of γ have the same probability to grow, two γ grains formed at neighboring locations in atrue-twin relationship, connecting with each other during growth. This can be also one mechanism of the cluster formation. Another possibility to explain the configuration found in Figure 8a is the simultaneous nucleation of differently oriented γ grains to reduce the strain anisotropy created by structural transformation. The interfaces between ω_o and γ are mostly semi-coherent with uniformly distributed dislocations analogous to that between the β_o and γ phase described in [14]. According to the synchrotron research from [13], the γ phase was expected toinitially have a coherent interface with the matrix while generally lost the coherency during growth. This seems also to apply in the present case despite the β_o phase has transformed to ω_o phase. In fact, according to our previous research, the growth of γ phase in the β_o matrix is much faster than that ofω_o phase at the beginning of aging [28]. Thus,it is considered that the major part ofγ phase stems from the $\beta_o \rightarrow \gamma$ transformation rather than a direct transition of$\omega_o \rightarrow \gamma$.However, the direct $\omega_o \rightarrow \gamma$ transformation cannot be ruled outduring further aging. Indeed, a

small number of small-sized and isolated γ grains are observed embedded within the ω_o phase. Finally, in Figure 8b, it should be noted that a group of dislocations are activated in the ω_o phase, which is not usually reported in the ωstructures. These dislocations seem to be generated from the ω_o/γ interface as evidenced in Figure 4c.

3.4 Effects of Ta, V and Zr on the microstructure and phase compositions at different temperatures

Small amounts (2 at.%) of Ta, V and Zr were added in the Ti_4Al_3Nb alloy substituting Ti to investigate their effects on the microstructure. Different from other elements such as Mo and Ni[15-16], these three elements seem not to have significant influence on the ω_o phase but all of them can stabilize β_o phase below 900 ℃. In the Ti_4Al_3Nb ternary alloy, the ω_o phase is stable at 900 ℃. This is in accordance with what is reported in other alloys, where the solvus temperature of ω_o phase was expected to be 870±40 ℃ or 913 ℃ [6, 39]. However, the published data is mostly obtained from two-phase TiAl alloys. In the present alloy with the nominal composition of ω_o, it is reasonable to speculate that the solvus of $\omega_o$phase is higher than 900℃. Figures 9 and 10 show the results after the 800 and 900 ℃aging treatment of the Ti_4Al_3Nb-2Ta, Ti_4Al_3Nb-2V and Ti_4Al_3Nb-2Zr alloys. Generally, the microstructures exhibit similar morphologies as the ternary alloy after aging. However, a common feature of the three alloys is that the β_o phase appears instead of ω_o phase in the sample aged at 900 ℃ while the ω_o phase still exists at 800 ℃, as evidenced by the SAD patterns in Figure 10. A few dislocations are discerned in the β_o matrix, which is probably because the dislocation glide in high temperature β_o phase is much easier than in the ω_o phase so that the emission of misfit dislocations is prone to happen at 900 ℃.

Table 1 summarizes the phase compositions in the three quaternary alloys as well as the base Ti_4Al_3Nb alloy. The partition ratio of Nb and the alloying elements between ω_o/β_o and γ phases are listed in the last column. For the ternary alloy, the ω_o and γ phase compositions are nearly constant in samples aged at 800 and 900 ℃ except for a slight decrease in the Nb ratio at 900 ℃. While γ as well as ω_o phase have higher Nb contents at 900 ℃,this decrease of the Nb ratio is most probably due to the increase ofNbsolubility is more pronounced for the γ phase. As a result, the volume fractions of the phases should change correspondingly. If the minor amount of α_2 phase is neglected, the volume fraction of ω_o phase should decrease while that ofγ phase increases to keep the average Nb content stable. Since the nominal composition of ω_o phase is Ti-37.5Al-12.5Nb, the extra Nb atoms probably substitute on the Ti atom sites. After the alloying elements are added, the Nb content in the ω_o phase behaves differently at different temperatures, indicating the alloying elements have slightly altered the phase equilibrium so that the volume fractions of ω_o/β_o and γ change accordingly. For each of the alloying elements, distinct conclusions can be drawn. In the Ta-containing alloy, although the partition ratio at 800 and 900 ℃ is different, the atomic contents in ω_o/β_o and γ phases in fact do not vary so much. In both ω_o and β_o phases the Ta contents are higher than that in the γ phase at the same temperature, suggesting a tendency of $\beta_o \approx \omega_o > \gamma$. However, this is not the case in the V-containing alloy, in which the V contents in the ω_o and

γ phases are nearly the same whereas a higher partition ratio is obtained at 900 ℃ for the β_o and γ phases, suggesting a preference of β_o>γ≈ω_o. In the Zr-containing alloy, a preferenceof partitioning to the γ phase is found at 800 ℃ whereas a ratio of 1.00 is found in the β_o+γ phase microstructure, suggesting a sequence of β_o≈γ>ω_o. In terms of the atomic site occupancy, based on the nominal composition of ω_o phase at 800 ℃ and the assumption that extra Nb atoms are located on the Ti sites, it can be expected that the Ta atoms prefer toreplaceTiatoms whereas V and Zrprefer toreplace Al atoms. For the β_o phase, the reverse substitution is deduced. From the atomic contents shown in Table 1, a general conclusion can be drawnthat even though all the elements Ta, V and Zr have a negative effect on the stability of the ω_o phase, the effect of Ta seems to be relatively weaker than that of V and Zr.

4. Conclusions

In this study, the microstructures of ω_o-Ti_4Al_3Nb type alloys after quenching and subsequent aging at various temperatures were examined by electron microscopy. The precipitation behavior of γ phase was investigated and the formation mechanisms of various interface structures were discussed. Finally, Ta, V and Zr elements were added to study their effects on the stability of ω_o phase. The main conclusions are summarized as follows:

1.The microstructure of the aged samples is mainly composed of elongatedγ grains in $<110>_\gamma$ directionsand ω_o matrix in the Ti_4Al_3Nb alloy. The microstructure is very fine-grained which is due to the multiple variant formation of the ω_o, γ and α_2 phases from the β_o matrixin different orientation relationships.

2. Various types of interfaces are formed based on the overall $\{11\bar{2}0\}_{\omega o}//\{0001\}_{\alpha 2}//\{111\}_\gamma$; $<0001>_{\omega o}//<11\bar{2}0>_{\alpha 2}//<101>_\gamma$orientation relationship. These interfaces are mostly semi-coherent due to the misfits between the phases. A number of stacking faults are found in the $\alpha_2$phase whichare considered as the nuclei of γ. The twin-like morphology of α_2 phase is also observed with a straight interface.

3. In the samples aged at 750 ℃ the γ phase mainly forms from the α_2 phase whereas in the samples aged at 800 and 900 ℃ the direct nucleation of multiple γ variants from the β_o and ω_o phases is more common, forming clusters of grains.

4. The microstructures of the Ta, V and Zr containing alloys are similar to that of the ternary alloy after the same aging experiments. All three elements have a negative effect on the stability of ω_o phasebutthe effect of Ta seems to be weaker than that of V and Zr.

Acknowledgments

This work was supported by the National Natural Science Foundation of China (contract Nos. 51971175, 51831001 and 51601146), State Key Lab of Advanced Metals and Materials (contract No. 2017-ZD02).

Li Wang acknowledges the financial support from the Helmholtz Association in the frame of Helmholtz Postdoc Program. Lin Song is grateful for the fruitful discussion with Dr. Ulrich Fröbel.

References

[1] F. Appel, J.D.H. Paul, M. Oehring. Gamma Titanium Aluminide Alloys: Science and Technology. Wiley-VCH, Weinheim, Germany, 2011.

[2] M. Schloffer, B. Rashkova, T. Schoberl, E. Schwaighofer, Z.L. Zhang, H. Clemens, S. Mayer. Evolution of the ω_o phase in a β-stabilized multi-phase TiAl alloy and its effect on hardness, Acta Mater. 64 (2014) 241-252.

[3] J. Ding, M.H. Zhang, Y.F. Liang, Y. Ren, C.L. Dong, J.P. Lin. Enhanced high-temperature tensile property by gradient twin structure of duplex high-Nb-containing TiAl alloy. Acta Mater.161 (2018) 1-11.

[4] Z.W. Huang. Ordered ω phases in a 4Zr–4Nb-containing TiAl-based alloy. Acta Mater. 56 (2008) 1689-1700.

[5] L. Song, X.J. Xu, J. Sun, J.P. Lin. Cooling rate effects on the microstructure evolution in the βo zones of cast Ti–45Al–8.5Nb–(W, B, Y) alloy. Mater. Character. 93 (2014) 62-67.

[6] A. Stark, M. Oehring, F. Pyczak, A. Schreyer. In situ observation of various phase transformation paths in nb-rich tial alloys during quenching with different rates. Adv. Eng. Mater. 13 (2011) 700-704.

[7] S. Bystrzanowski, A. Bartels, A. Stark, R. Gerling, F.P. Schimansky, H. Clemens. Evolution of microstructure and texture in Ti-46Al-9Nb sheet material during tensile flow at elevated temperatures. Intermetallics 18 (2010) 1046-1055.

[8] T. Ye, L. Song, Y.F. Liang, M.H. Quan, J.P. He, J.P. Lin. Precipitation behavior of ω_o phase and texture evolution of a forged Ti-45Al-8.5Nb-(W, B, Y) alloy during creep. Mater. Character.136 (2018) 41-51.

[9] J. Lapin, T.Pelachová, V.T.Witusiewicz, E.Dobročka. Effect of long-term ageing on microstructure stability and lattice parameters of coexisting phases in intermetallic Ti–46Al–8Ta alloy. Intermetallics 19 (2011) 121-124.

[10] V.T. Witusiewicz, A.A. Bondar, U. Hecht, T.Y. Velikanova. The Al–B–Nb–Ti system IV. Experimental study and thermodynamic re-evaluation of the binary Al–Nb and ternary Al–Nb–Ti systems. J. Alloys Compds. 472 (2009) 133-161.

[11] L. Song, X.J. Xu, L. You, Y.F. Liang, J.P. Lin. Ordered ω phase transformations in Ti-45Al-8.5Nb-0.2B alloy. Intermetallics 65 (2015) 22-28.

[12] T.T. Cheng, M.H. Loretto. The decomposition of the beta phase in Ti–44Al–8Nb and Ti–44Al–4Nb–4Zr–0.2Si alloys. Acta Mater. 46 (1998) 4801-4819.

[13] P. Erdely, P. Staron, A. Stark, T. Klein, H. Clemens, S. Mayer. *In situ* and atomic-scale investigations of the early stages of γ precipitate growth in a supersaturated intermetallic Ti-44Al-7Mo (at.%) solid solution. Acta Mater. 164 (2019) 110-121.

[14] L. Song, X.G. Hu, T.B. Zhang, J.S. Li. Precipitation behaviors in a quenched high Nb-containing TiAl alloy during. Intermetallics 89 (2017) 79–85.

[15] T. Klein, M. Schachermayer, D. Holec, B. Rashkova, H. Clemens, S. Mayer. Impact of Mo on the ω_o phase in β-solidifying TiAl alloys: An experimental and computational approach. Intermetallics 85 (2017) 26-33.

[16] L. Song, J.P. Lin, J.S. Li. Effects of trace alloying elements on the phase transformation behaviors of ordered ω phases in high Nb-TiAl alloys. Mater. Des. 113 (2017) 47–53.

[17] L. Song, X.J. Xu, L. You, Y.F. Liang, J.P. Lin.Phase transformation and decomposition mechanisms of the $\beta_o(\omega)$ phase in cast high Nb containing TiAl alloy. J. Alloys Compds. 616 (2014) 483–491.

[18] Z.W. Huang. Thermal stability of Ti-44Al-4Nb-4Hf-0.2Si-1B alloy. Intermetallics 37 (2013) 11-21.

[19] Z.W. Huang. Thermal stability of Ti-44Al-4Nb-4Zr-0.2Si-1B alloy. Intermetallics42 (2013) 170-179.

[20] H. Jiang, D. Hu, X. Wu. Thermal stability of the omega phase in Zr-containing TiAl alloys. J. Alloys Compds. 475 (2009) 134-138.

[21] L.A. Bendersky, W.J. Boettinger, B.P. Burton, F.S.Biancaniello, C.B.Shoemaker. The formation of ordered ω-related phases in alloys of composition Ti_4Al_3Nb. Acta Metall. Mater. 38 (1990) 931-943.

[22] T. Ye, L. Song, M.H. Quan, J.P. He, J.P. Lin. Precipitation behavior of ω_o phase in Ti-37.5Al-12.5Nb alloy. Metals7 (2017) 192.

[23] L. Song, J.P. Lin, T.B. Zhang, J.S. Li. Precipitation behavior of α_2 phase in Ti-34Al-13Nb alloy. J. Alloys Compds. 5 (2017) 155-162.

[24] A.Denquin, S. Naka. Phase transformation mechanisms involved in two-phase TiAl-based alloys—I. Lambellar structure formation. Acta Mater. 44 (1996) 343-352.

[25] K.Kishida, H. Inui, M. Yamaguchi. Deformation of lamellar structure in TiAl-Ti3Al two-phase alloys. Philo. Mag. A 78 (1998) 1-28.

[26] S. Nag, R. Banerjee, R. Srinivasan, J.Y. Hwang, M. Harper, H.L. Fraser. ω-Assisted nucleation and growth of a precipitates in the Ti–5Al–5Mo–5V–3Cr–0.5Fe βtitanium alloy.Acta Mater. 57 (2009) 2136–2147.

[27] R. Banerjee, D.Bhattacharyya, P.C. Collins, G.B. Viswanathan, H.L. Fraser. Precipitation of grain boundary α in a laser deposited compositionally graded Ti–8Al–*x*V alloy – an orientation microscopy study. Acta Mater.52 (2004) 377-385.

[28] L. Song, J.P. Lin, J.S. Li. Phase transformation mechanisms in a quenched Ti-45Al-8.5Nb-0.2W-0.2B-0.02Y alloy after subsequent annealing at 800 °C. J. Alloys Compds.691 (2017) 60-66.

[29] L.C. Zhang, M. Aindow. Morphology and interfacial structure of gamma precipitates in the beta phase of a Ti-Al-Nb-Zr alloy. J. Mater. Sci. 41 (2006) 611-619.

[30] E. Lee, R. Banerjee, S. Kar, D. Bhattacharyya, H. L. Fraser. Selection of α variants during microstructuralevolution in α/β titanium alloys. Philos. Mag A 87 (2007) 3615–3627.

[31] F. Appel. Mechanistic understanding of creep in gamma-base titanium aluminide alloys. Intermetallics 9 (2001) 907-914.

[32] F. Appel. Mechanistic understanding of creep in gamma-base titanium aluminide alloys. Mater. Sci. Eng. A 317 (2001) 115-127.

[33] J.P. Simmons, M.J. Mills, S.I. Rao. Structure of 1/2<110> Dislocations in γ-Tial by high resolution TEM and embedded atom method modelling. MRS Proceedings, 364(1994) 137.

[34] L. Song, X.J. Xu, L. You, Y.F. Liang, Y.L. Wang, J.P. Lin. Ordered α_2 to ω_o phase transformations in high Nb containing TiAl alloys. Acta Mater. 91 (2015) 330-339.

[35] S.A. Court, J.P.A. Löfvander , M.H. Lorettom H.L. Fraser. The influence of temperature and alloying additions on the mechanisms of plasticdeformation of Ti_3Al. Philos. Mag A 61 (1990) 109-139.

[36] M. Musi, P. Erdely, B. Rashkova, H. Clemens, A. Stark, P. Staron, N. Schell, S. Mayer. Evidence of an orthorhombic transition phase in a Ti-44Al-3Mo (at.%) alloy using *in situ* synchrotron diffraction and transmission electron microscopy. Mater. Character. 147 (2019) 398-405.

[37] L. Song, L. Wang, M. Oehring, X.G. Hu, F. Appel, U. Lorenz, F. Pyczak, T.B. Zhang. Evidence for deformation twinning of the $D0_{19}$-α_2 phase in a high Nbcontaining TiAl alloy. Intermetallics109(2019) 91–96.

[38] J.W. Lee, S. Hanada, M.H. Yoo, Deformation twinning systems of $D0_{19}$ structured Ti-34mol%Al, Scripta Metall. Mater. 33 (1995) 509–514.

[39] H.F. Chladil, H. Clemens, G.A. Zickler, M. Takeyama, E. Kozeschnik, A. Bartels, T. Buslaps, R. Gerling, S. Kremmer, L.A. Yeoh, K.-D. Liss. Experimental studies and thermodynamic simulation of phase transformations in high Nb containing γ-TiAl based alloys. Int. J. Mater. Res. 98 (2007) 1131-1137.

Table 1 The phase composition and partition ratios of alloying elements obtained by EDX

Heat treatment	Alloy	Phase	Ti	Al	Nb	Ta	V	Zr	Partition ratio ($\frac{\omega_o}{\gamma}$ or $\frac{\beta_o}{\gamma}$)
800 °C/100 h	Ti_4Al_3Nb alloy	ω_o	48.3±0.9	37.8±0.8	13.9±0.5	-	-	-	Nb: 1.60
		γ	40.2±0.8	51.1±1.2	8.7±0.4	-	-	-	
	2Ta-alloy	ω_o	46.1±0.9	37.1±0.5	15.1±0.4	1.7±0.1	-	-	Nb: 1.68
		γ	39.7±1.0	50.7±1.2	9.0±0.4	0.6±0.1	-	-	Ta: 2.83
	2V-alloy	ω_o	47.5±1.2	36.5±1.6	14.7±0.4	-	1.3±0.0	-	Nb: 1.58
		γ	39.9±1.0	49.5±1.2	9.3±0.4	-	1.2±0.2	-	V: 1.08
	2Zr-alloy	ω_o	48.1±0.5	34.9±0.5	15.2±0.1	-	-	1.8±0.0	Nb: 1.62
		γ	40.6±0.5	47.2±0.5	9.4±0.1	-	-	2.8±0.0	Zr: 0.64
900 °C/100 h	Ti_4Al_3Nb alloy	ω_o	47.9±1.4	37.3±0.8	14.8±0.7	-	-	-	Nb: 1.54
		γ	40.9±0.9	49.5±1.1	9.6±0.2	-	-	-	
	2Ta-alloy	β_o	48.1±1.3	35.8±1.4	14.5±0.2	1.6±0.1	-	-	Nb: 1.44
		γ	40.0±0.8	49.2±1.2	10.1±0.4	0.7±0.1	-	-	Ta: 2.29
	2V-alloy	β_o	45.8±0.3	38.5±0.4	13.7±0.3	-	2.0±0.1	-	Nb: 1.46
		γ	38.5±1.1	51.3±1.4	9.4±0.3	-	0.8±0.1	-	V: 2.50
	2Zr-alloy	β_o	45.7±0.5	38.4±1.3	13.8±0.8	-	-	2.1±0.1	Nb: 1.52
		γ	38.7±0.8	50.1±1.3	9.1±0.4	-	-	2.1±0.1	Zr: 1.00

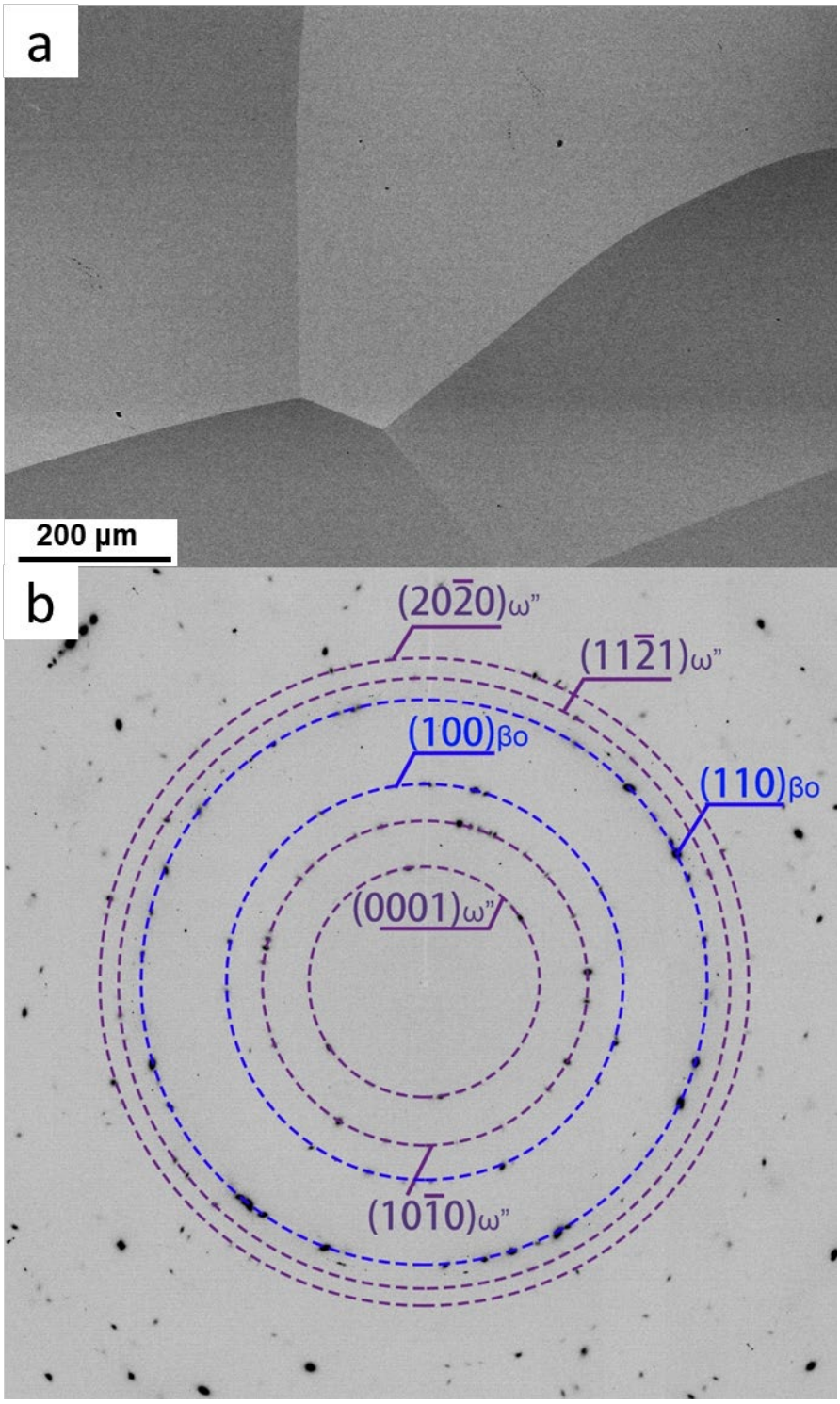

Figure 1 (a) SEM-BSE image of the Ti_4Al_3Nb alloy after quenching from 1250 °C; (b) synchrotron radiation X-ray diffraction pattern of the as-quenched material

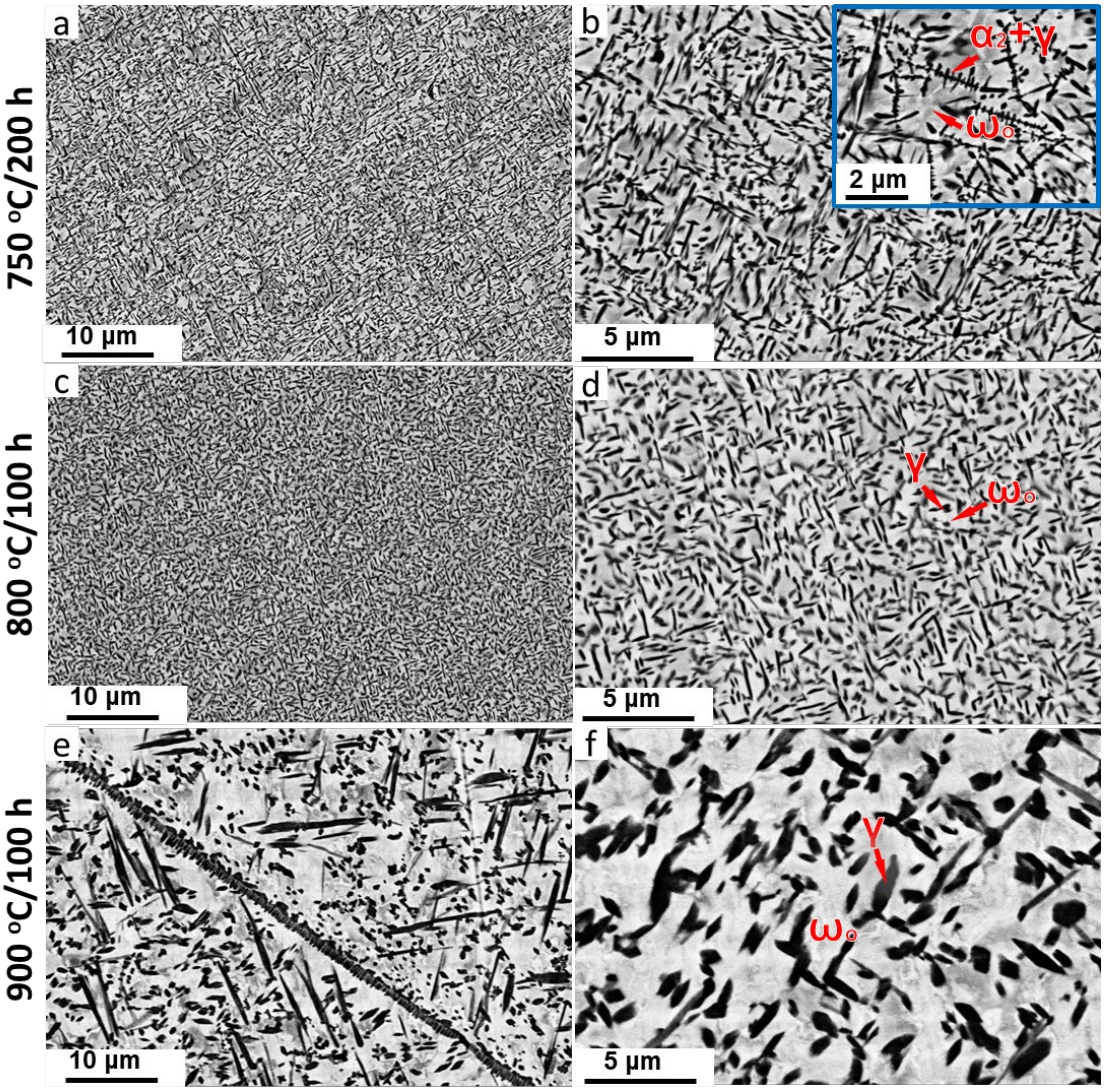

Figure 2 SEM-BSE images of the microstructure after annealing at 750 °C (a-b), 800 °C (c-d) and 900 °C (e-f). Fine-grained microstructures mainly composed of γ and ω_o phases formed. Fish-bone like structure caused by γ phase coarsening from α_2 laths are observed at 750 °C whereas at 800 and 900 °C the γ phase mainly precipitates directly from the matrix.

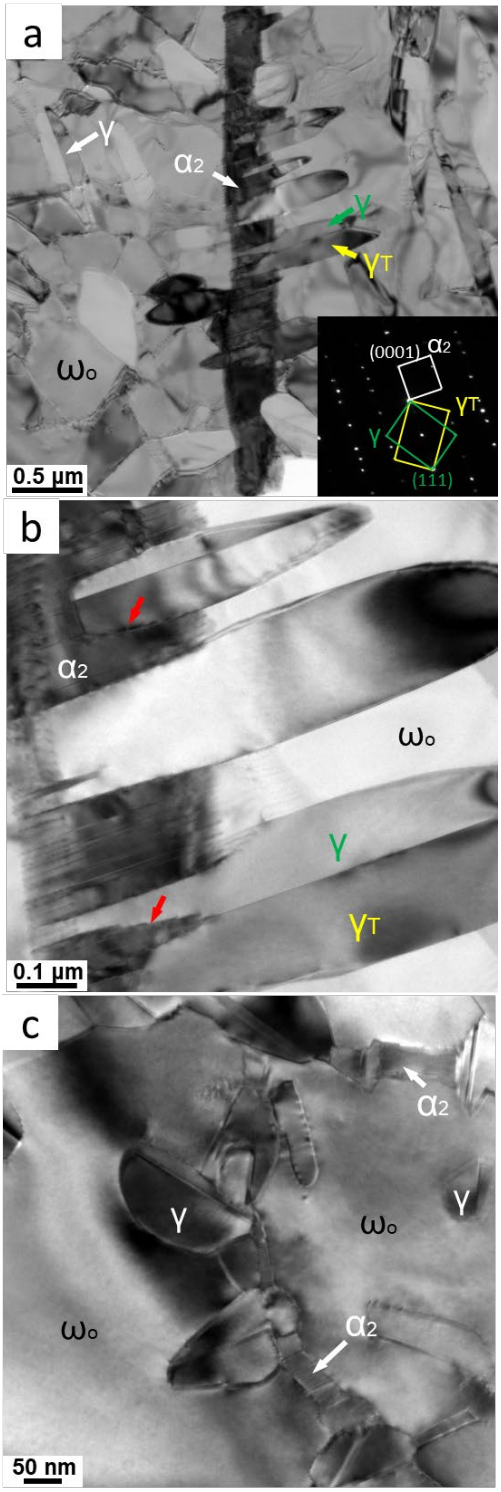

Figure 3 TEM images of the γ grains developed from the α_2 phase after annealing at 750 °C for 200 h: (a) grain boundary α_2 phase with coarsened γ grains in twin relationship; (b) enlarged image of (a), note the ledges at the γ/α_2 interfaces; (c) TEM image of a transformed α_2 phase in the ω_o matrix, the γ phase has formed in twin relationship.

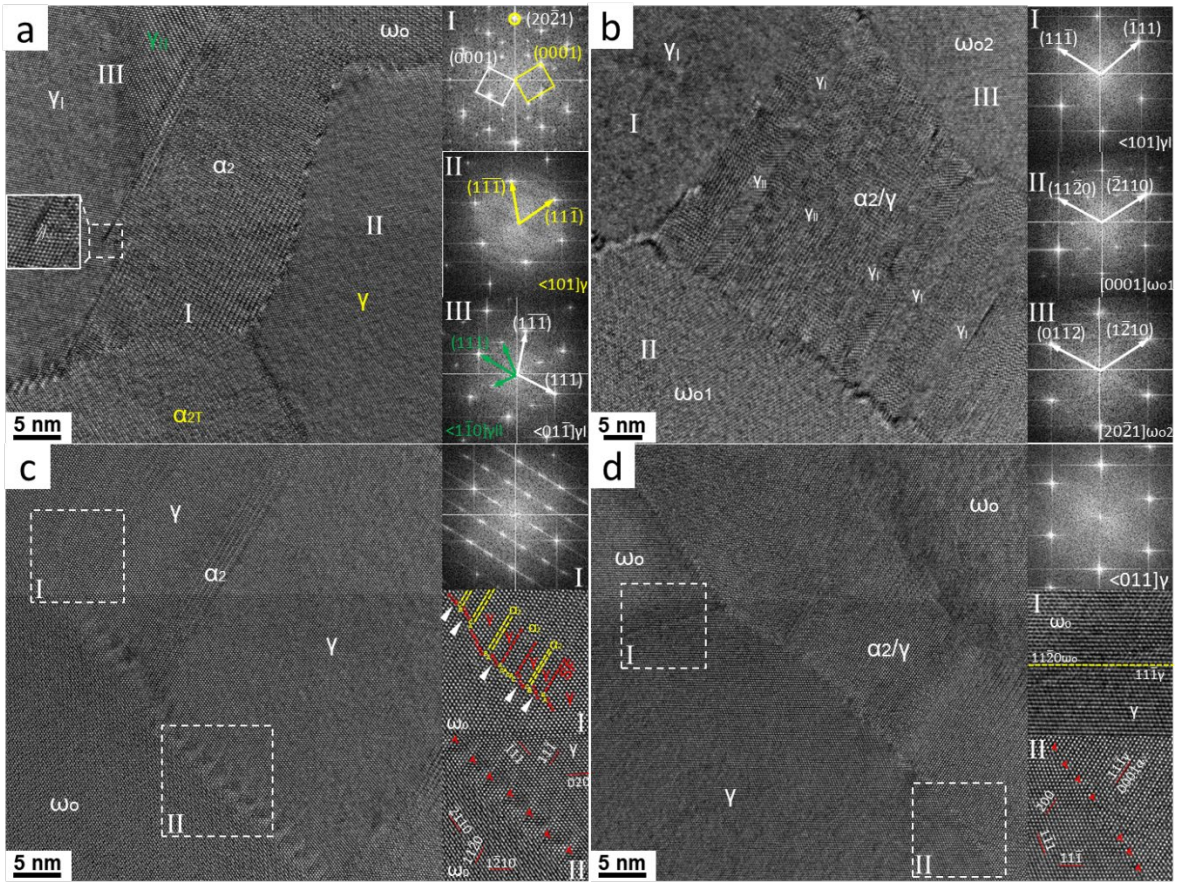

Figure 4 HRTEM images of the interfaces and the corresponding FFT patterns in the sample annealed at 750 ℃/200 h; magnified images of areas marked in pictures are shown as inserts: (a) two α_2 grains in a twin-like orientation relationship with γ phase formation in each of them; (b) numerous thin γ laths form inside α_2 with most of them in the same orientation; (c) semi-coherent interface formed between the transformed γ laths and the surrounding ω_o, an array of misfit dislocations is formed and a high density of stacking faults can also be observed; (d) a γ grain grown from the ω_o matrix, forming a continuous interface with ω_o whereas an interface with numerous misfit dislocations is formed with the lamellar structure.

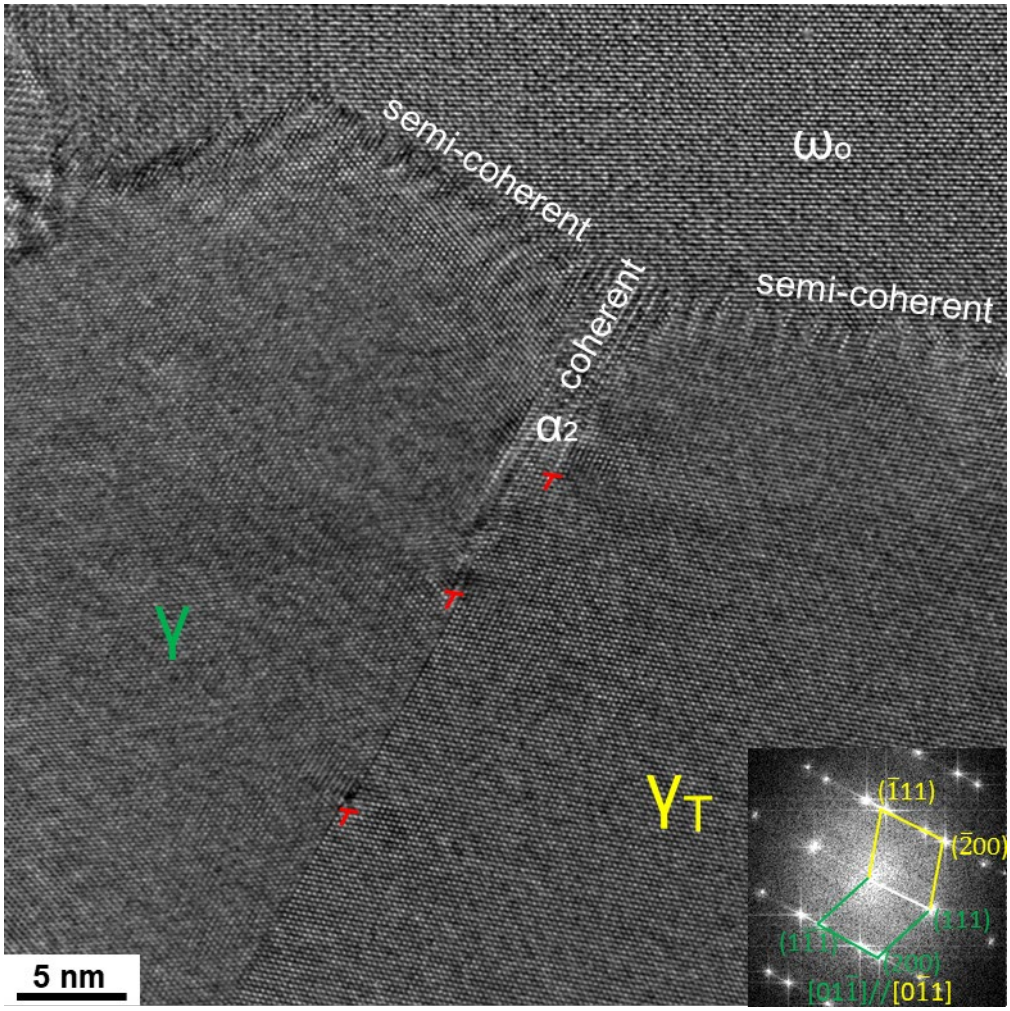

Figure 5 HRTEM image of a pair of γ twins formed from the α_2 phase in the sample annealed at 750 °C/200 h. A few ledges remained at the twinning interface and semi-coherent boundaries are formed between γ grains and ω_o phase.

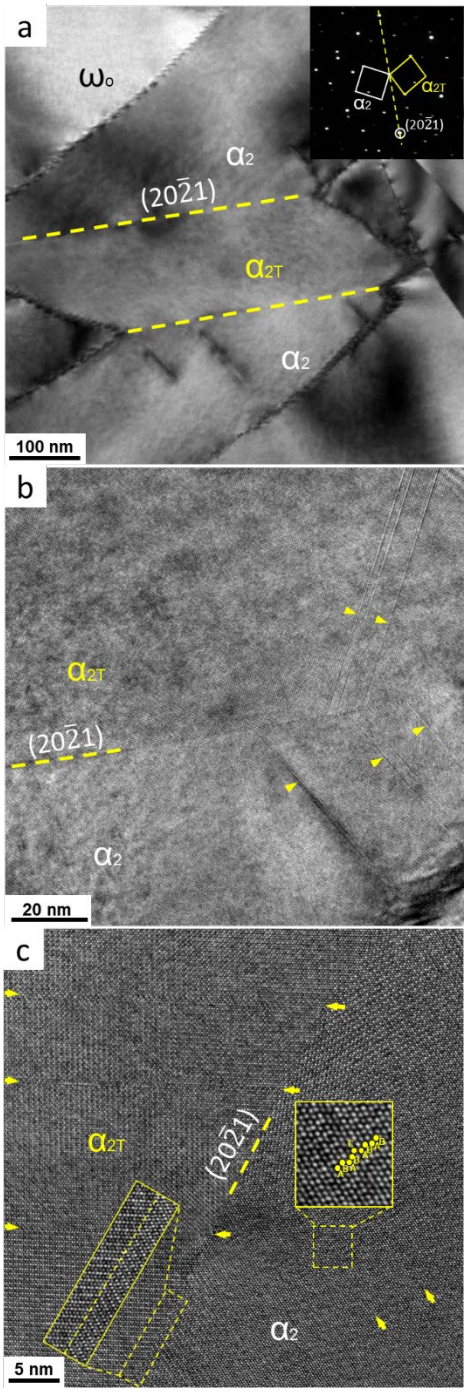

Figure 6 TEM (a) and HRTEM (b-c) images of the twin morphology of α_2 phase in the 750 °C/200 h annealed sample: A flat (20$\bar{2}$1) mirror plane and a number of stacking faults are observed.

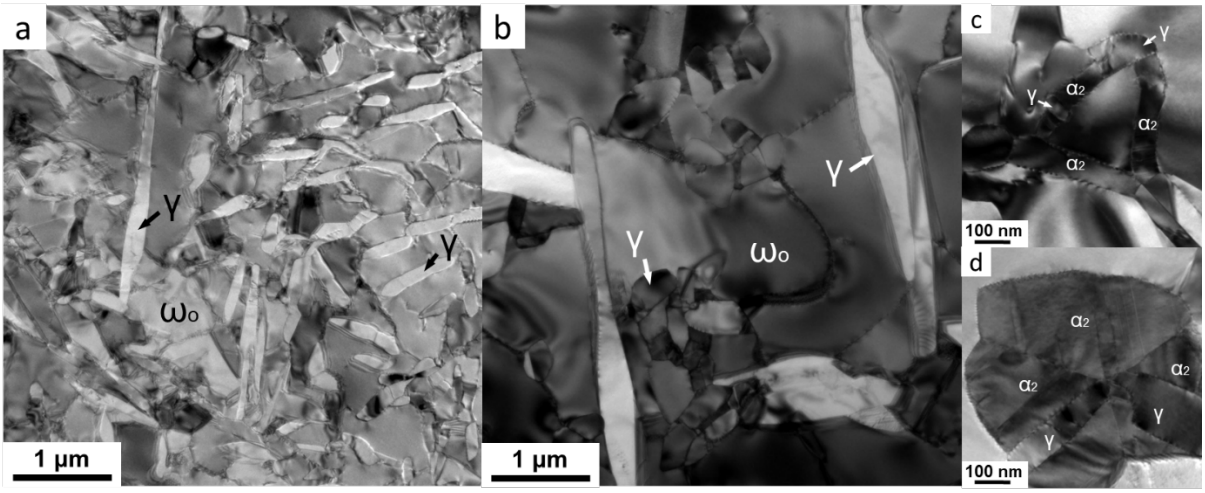

Figure 7 TEM images of the Ti_4Al_3Nb alloy annealed at 800 ℃ (a) and 900 ℃ (b-d) for 100 h after quenching from 1250 ℃.

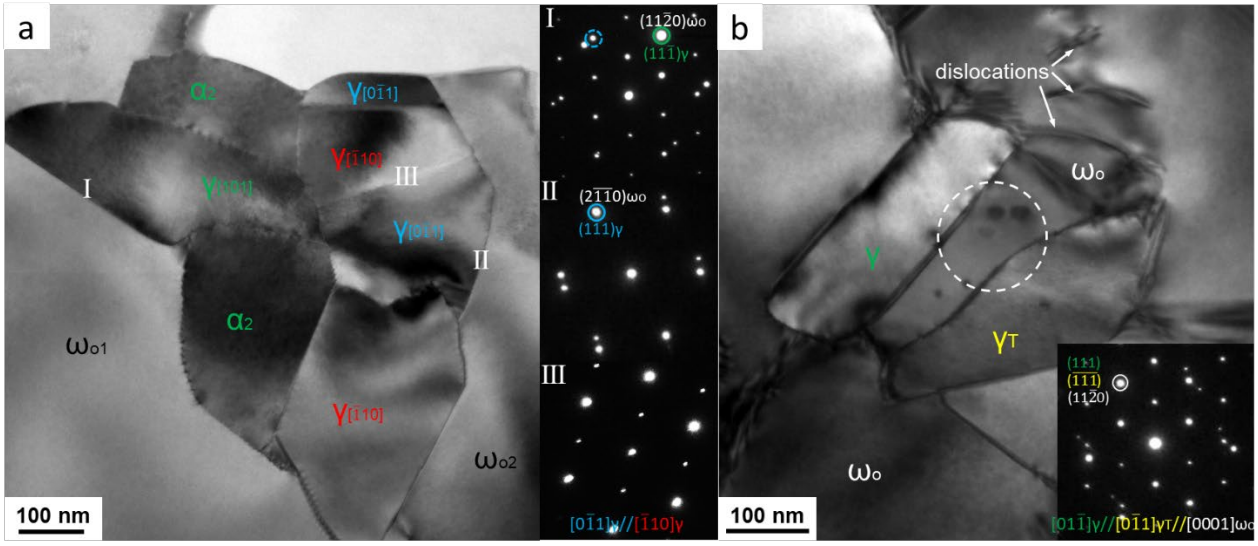

Figure 8 TEM image of a cluster of γ and α_2 grains (a) and two γ grains (b) formed in the ω_o matrix after annealing at 900 °C for 100 h. The SAD patterns obtained along different zone axes indicate that γ grains precipitate under $\{11\bar{2}0\}_{\omega o}//\{111\}_{\gamma}$; $[0001]_{\omega o}//<110>_{\gamma}$ orientation relationship whereas distinct orientation relationships between the γ grains were formed.

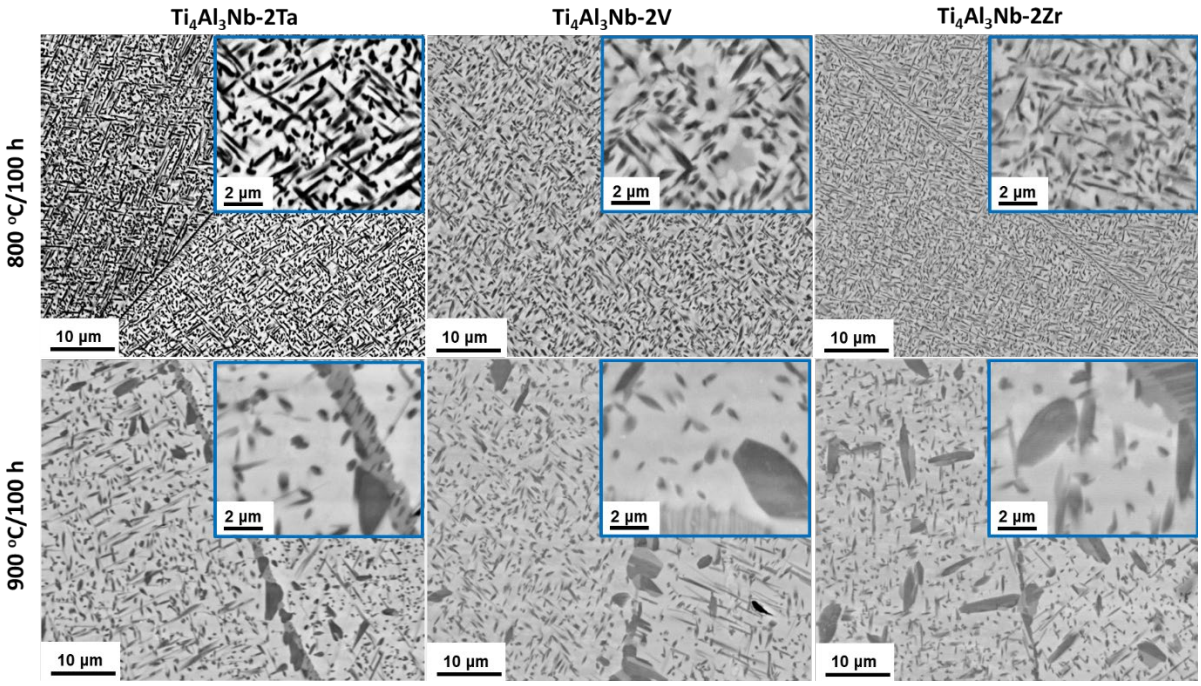

Figure 9 SEM images of the microstructures obtained in the Ta, V and Zr containing alloys at 800 and 900 °C. The morphologies are similar between different alloys at the same temperature.

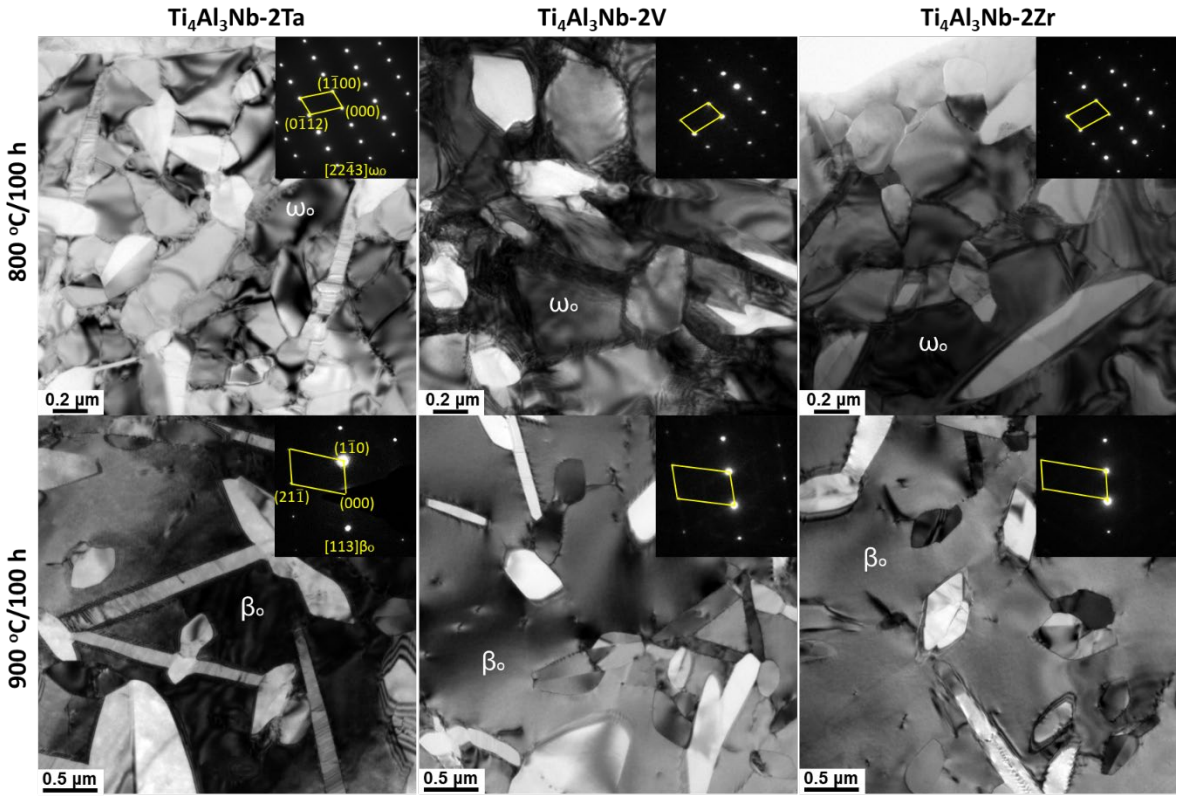

Figure 10 TEM images of the microstructures obtained in the Ta, V and Zr containing alloys at 800 and 900 °C. The matrix is composed of ω_o phase variants at 800 °C while of pure β_o phase at 900 °C.